7th International Conference on Modelling and Simulation in Nuclear Science and Engineering (7ICMSNSE)
Ottawa Marriott Hotel, Ottawa, Ontario, Canada, October 18-21, 2015

7ICMSNSE-xxx

Atomistic Modelling of Aqueous Systems Relevant to the SCWR

D. Kallikragas[1], I. Svishchev[1]
[1]Trent University, Peterborough, Ontario, Canada
dimitrioskallikragas@trentu.ca, isvishchev@trenut.ca

Abstract

Atomistic modelling is ideal for the study of corrosion phenomena, particularly at the extreme conditions of the Supercritical Water Cooled Reactor (SCWR). Understanding the behavior of supercritical water and species such as chloride and oxygen is needed for developing a corrosion control strategy. Molecular Dynamics simulations have been employed to study the properties of aqueous systems in nanometer-spaced iron hydroxide surfaces. Atomic density profiles as well as diffusion coefficients and hydration numbers within these surfaces are provided. These surface configurations simulate the environment of proto-cracks in the passivation layer of components in the SCWR.

Keywords: Effect of confinement, diffusion, density profiles, molecular dynamics simulations

1. Introduction

Of major concern in the design of the SCWR or any other SCW water technology is in choosing appropriate materials that can withstand the harsh environment imposed by water at supercritical conditions. Iron hydroxide is a corrosion product when iron based alloys are subjected to SCW and the brucite crystal structure is typical of many mineral structures. The behavior of water and aqueous species at this corrosion layer interface must be understood in order to predict general corrosion processes such as embrittlement, pitting corrosion and stress corrosion cracking [1-4].

Much experimental work has been done to measure the corrosion rates of alloys and ceramic materials in an environment representative of that expected in a SCWR core [5]. Identifying a fuel cladding material is the most challenging materials issue as the fuel cladding is exposed to a combination of very high temperature and pressure, plus the effects of irradiation on both the alloy and the coolant [6]. Stainless steel and nickel based alloys are both potential candidates for the fuel cladding and pressure tubes, due to their structural strengths and their resistance to corrosion [6]. Current and past experience indicates that although ferritic-martensitic steels exhibit the least susceptibility toward SCC, they tend to undergo the worst degree of oxidation in SCW. Nickel based alloys and austenitic steels experience a lesser degree of oxidation but are more likely to suffer from SCC [7]. Current practice in the chemistry control of fossil burning pants, is to add small amounts of oxygen to the feed water to promote the formation of hematite in between magnetite grain boundaries, which reduces the oxidation rate by inhibiting the diffusion of oxygen through the oxide film [7]. The formation of low solubility oxide and hydroxide layers provides a barrier to the diffusion of reactants from the coolant to the alloy surface, and protects the alloy from further oxidation.

Staehle et al. [8] carried out a detailed assessment of current and past research and operating experience on SCC from early 1950s until the present, and predicted that aging will result in significant changes in grain boundary chemistry and structure in SCWR in-core materials, leading to changes in SCC susceptibility. Testing during the US nuclear reheat development program in the 1960s found that chloride deposition eventually led to failure of austenitic stainless steel fuel cladding alloys by SCC. It was suggested that in situations where cracking was observed, deposition of moisture on the outer surface and subsequent evaporation may have led to chloride concentration on the surface.

Oxygen gas is a radiolytic by-product produced in the interaction of radiation with the coolant water, and the accumulation of oxygen in the system poses challenges in terms of the degradation of reactor materials through oxidation [9]. The diffusion coefficients of oxygen are required for the prediction of diffusion controlled reaction rates [10] and its influence on the water structure within the corrosion crevices, as well as hydration numbers are all relevant in the formulation of a corrosion control strategy. Wright and Dooley conducted a comprehensive review of the oxidation of alloys by high pressure steam for the potential use in steam boilers [11], and state that the initial rate of oxide formation is dependent on the partial pressure of the oxygen gas being greater than the dissociation oxygen partial pressure of the oxide. Once the oxide layer is established on the alloy surface, the rate of oxidation slows and becomes a function of the diffusion of oxidizing species across the oxide layer or by dissociation of oxides at the interface [11].

Viewed from the atomistic perspective, molecular dynamics (MD) simulations have now become a viable and time effective method for providing detailed information of the reaction dynamics of water and solvated species at high temperature and supercritical conditions. The Simple Point Charge-Extended (SPC/E) water model has been found to accurately reproduce physical and thermodynamic properties, including self-diffusion coefficients, over a wide range of temperatures and pressures [12, 13]. The SPC/E model provides through the principle of corresponding states, accurate thermodynamic behavior of water, particularly at high temperatures and in the supercritical region. Plugatyr used the SPC/E model to obtain an accurate dielectric equation of state for high temperature water as well ion pair association constants for LiOH in SCW [14, 15]. We have also used MD methods to parameterize an equation that gives accurate diffusion coefficients for oxygen and other radiolytic products in high temperature and SCW [16]. The more recently developed Clay Force Field (CLAYFF) has been used successfully to model the interaction energies of amorphous solids, oxides, layered hydroxides and interfacial systems [17, 18]. Classical MD simulations have been used to simulate a chloride ion as well as molecular oxygen in nanometer spaced $Fe(OH)_2$ surfaces at both high temperature, sub-critical water as well as at supercritical conditions. These surface configurations were intended to simulate the environment expected at crack tips of the $Fe(OH)_2$ corrosion layer in the SCWR.

2. Computational Methods

Two electrostatically neutral $Fe(OH)_2$ surfaces were created by cleaving the equilibrated brucite crystal structure, at 298 K and 1 bar pressure, along the interlayer (0 0 1) plane and the OH groups were left intact. The simulation cell thus contained two crystalline slabs comprised of two $Fe(OH)_2$ sheets each, consisting of a total of 72 Fe atoms and 144 OH groups per slab, with 36 OH groups, or equivalently, 36 unit cells of the brucite structure on each side of the gap exposed to the water. The slabs had the dimensions of 19.5917 × 16.9669 × 9.2082 Å, with an additional 10, 20 and 80 Å added in the z-direction to account for the gaps for each configuration. Density was estimated from the

atomic mass of water molecules within the geometric volume of confinement between the surfaces [19]. State points were chosen to mimic coolant conditions in the heat transports system of the SCWR and included the following pairs: 0.620 g cm^{-3} and 567 K, 0.093 g cm^{-3} and 715 K, 0.067 g cm^{-3} and 814 K, and both 0.044 and 0.055 g cm^{-3} at 913 K. The equations of motion were integrated using the Verlet Leap-Frog algorithm with a time step ranging from 0.5 to 1 fs [20]. An NVT ensemble was used, meaning the number of molecules, simulation cell volume and temperature were kept constant, and the temperature was maintained using the Nose–Hoover thermostat [21]. Periodic boundary conditions were employed and the atomic pair interactions were calculated using the Lorentz–Berthelot mixing rules, with a spherical cut off radius set at half the length of the smallest side of the simulation cell. Long-range Coulombic interactions were handled via the Ewald Summation method [20]. Intermediate averaging was performed every 1 ps and the simulations were allowed to proceed for a total time of 5 ns. For the infinitely dilute, bulk water simulations, 1 oxygen molecule or 1 chloride ion, and 500 waters were simulated, also with a 5 ns trajectory. The SPC/E water potential used was taken from Berendsen et al. [22] , the OH potential was taken from Wiener et al. [23], the CLAYFF force field for Fe was taken from Cygan et al. [17] and the oxygen potential was taken from Hansen, Agbor and Kiel. [24] The simulations were performed on the Shared Hierarchy Academic Resource Computing Network (SHARCNET), a consortium of Ontario universities and colleges operating a network of high performance computer clusters.

3. Results

3.1 Radial distribution functions

Figure 1 shows the radial distribution functions (RDF's) for oxygen – water, and chloride – water pairs, for both the bulk water systems, and with 10 Å of surface separation for the 567 K, 0.620 g cm^{-3}, and for bulk water and 80 Å of surface spacing for the 913 K, 0.044g cm^{-3} system. Figure 1a) shows the centre of mass of the oxygen molecule to the oxygen atom of the solvating water (COM – O_w), and b) shows the oxygen atom of the molecule to a hydrogen atom of water (O – H_w). Figure 1c) shows the RDF for the chloride and oxygen atom of the water (Cl^- - O_w), and d) shows the chloride ion and hydrogen atom of the neighbouring water (Cl^- - H_w). These Pair Correlation Functions give the probability of finding an atom of the solvent molecule at a given distance from the solute and provide insights into the organization of the solvent molecules and hydrogen bonding within the gap. These RDF's were chosen to represent the two extremes of high density and small confinement and low density with least confinement. For brevity, they were chosen to illustrate the effect of the solute as well as that of confinement on the water at 10 Å and how it is absent at 80 Å of surface separation. This result is supported by the density profiles discussed below.

From the Figure 1a), the first minimum in all systems occurred on average at 5.0 Å with a peak at 3.5 Å, indicating that the solvation shell of waters around the O_2, extends to a distance of 5 Å from the COM of the oxygen, with the greatest extent of solvating waters being oriented at 3.5 Å. A large peak is seen for the 567 K system spaced at 10 Å, indicative of the ordering of the waters in this spacing, as shown in the density profiles in Section 3.3.

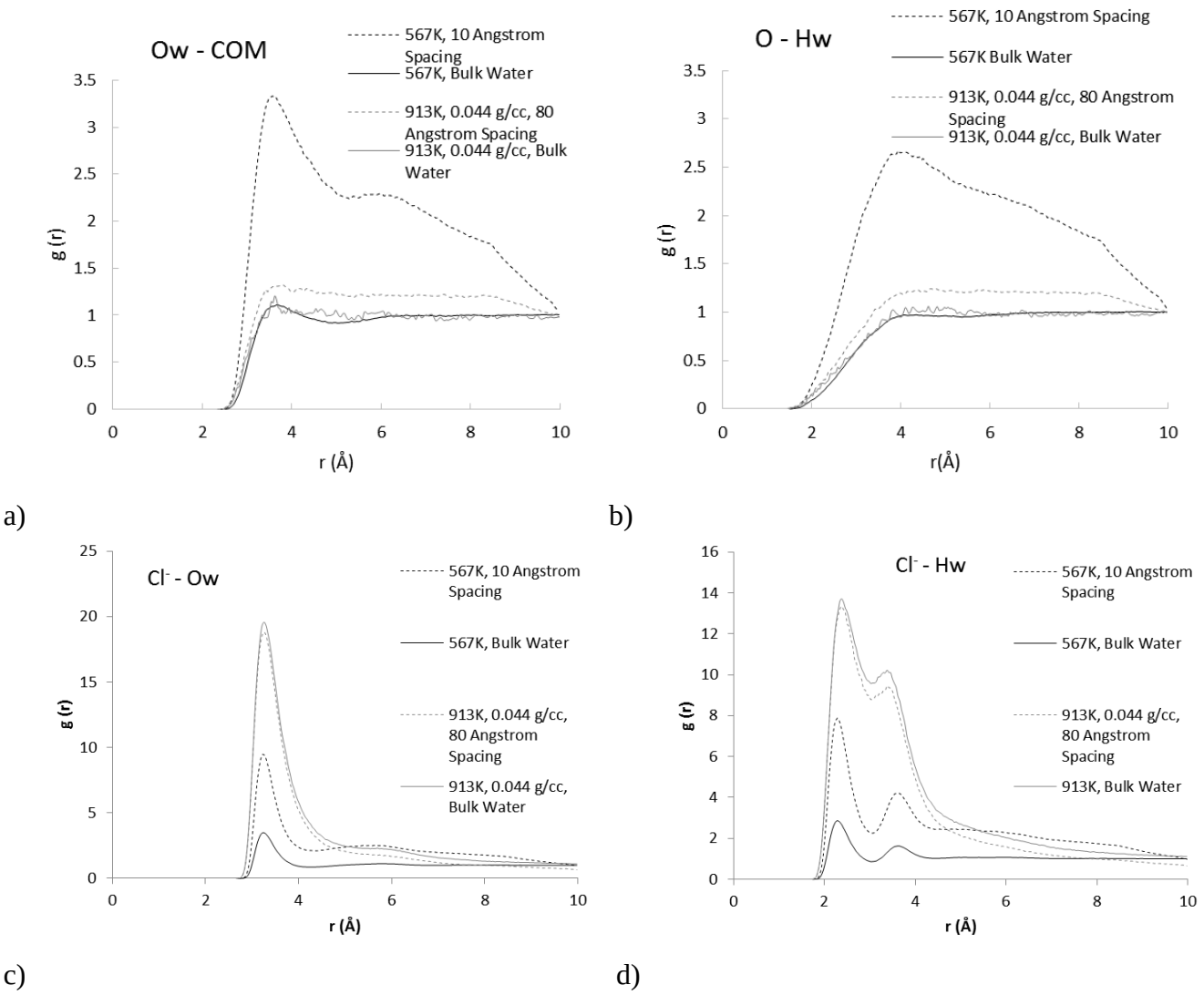

Figure 1 Radial Distribution Functions for oxygen-water and chloride-water pairs. a) Centre of mass of oxygen molecule to oxygen atom of water; b) Oxygen atom of O_2 molecule to the hydrogen atom of water; c) Chloride to oxygen atom of water and d) Chloride to hydrogen atom of water

This peak is greatly diminished in the 913 K system, with the RDF being very close to the bulk value. Both COM – O_w plots for the bulk values, are identical, and reach a peak of just over 1, indicating that in the unconfined system there is little preferential water structure around the O_2.

From the O – H_w RDF shown in b), a similar large peak is seen in the 567 K, 10 Å system with the 913 K, 80 Å system approaching that of the bulk water simulations. Again, both 567 and 913 K bulk water RDF's are nearly identical, with maximum values of 1, further suggesting there is no ordering of the waters around the O_2 in the unconfined system. There is no evidence of hydrogen bonding between the O_2 and the water, and any O – H_w interaction is a weak polar attraction of the slightly positive H atom of the water, and the instantaneous dipole moment of the O_2.

In Figure 1 c), the radial distribution functions for the Cl^- - O_w pairs for 567 and 913 K bulk water-chloride systems show the first coordinated shell of water molecules around the chloride ion to lie

within a distance of 3 to 3.75 and 3 to 4.3 Å, respectively. The first peak in the Cl^- - O_w correlation is observed at around 3.25 Å which remained relatively constant for all systems. It can be seen from the Cl^--O_w RDF for the 567 K systems that the peak height increases when the water is confined between the $Fe(OH)_2$ surfaces spaced at 10 Å apart. Again as seen for oxygen, both RDFs for the bulk and 80 Å surface spacing at 913 K and 0.044 g cm^{-3} are identical, suggesting there is little effect when the gap size reaches this distance. There is no appreciable ordering of waters beyond this distance as the curves are flat beyond this range.

For the Cl^--H_w pair distributions shown in Figure 1 d), a distinct maximum corresponding to hydrogen bonded waters is observed at around 2.3 Å that was consistent in all of the systems, both bulk and confined. A second, less pronounced peak in probability is observed outwards to around 3.75 Å, which corresponds to hydrogen atoms of coordinated water molecules not directly bonded to Cl^- (i.e. reflecting H-O-H···Cl^- pairs). Beyond this second peak, the RDF falls off steadily with no indication of any ordering at distances greater than 4.75 Å. There is essentially no change seen in the Cl^--H_w RDF's at 913 K when moving from the bulk systems to those confined between the $Fe(OH)_2$.

3.2 Coordination numbers

Table 1 shows the O_2 - water and water - water hydration numbers for all systems studied. Coordination numbers for the O_2 molecule, chloride ion and water – water pairs, were obtained by integrating the radial distribution functions (RDF's) to the first minimum.

Little variation is seen in the densest, 567 K, 0.620 g cm^{-3} systems, with the total water coordination around the O_2 ranging from 7.45 at 10 Å to 7.78 at 80 Å. As the density decreases, more varied hydration numbers are seen, increasing by as much as 50 % from in the 913 K systems when comparing 10 and 80 Å. In all cases, the total water hydration as defined by water oxygens around the centre of mass of the O_2 molecule at 80 Å approaches that seen in bulk water.

The total number of water-hydrogen atoms oriented around the oxygen atom of the O_2, show similar results as the COM - O_w discussed above. The O_{oxygen} - H_w coordination numbers show that the majority of the waters around the O_2 are oriented around the oxygen atoms. Little variation is seen in the subcritical system, which can be attributed to the higher density of these systems forcing more waters close to the O_2, resulting in a less varied numbers of waters in the solvation shell. As the system density decreases, the variation becomes more pronounced, with a similar increase of just under 50 % at 913 K, comparable to the COM - O_w coordination numbers.

More pronounced differences are seen in the water – water hydration numbers, with a 50 % increase in the number of solvating waters seen at as low a temperature as 715 K. This ratio increases to 100 % more solvating waters in the 913 K, 0.044 cm^{-3} simulations. There was little variation seen in the number of hydrogen bonds formed between the water – water pairs, with the two temperatures nearest the critical point of bulk water, 567 and 715 K, having hydrogen bond lengths of 2.42 Å, which decreased slightly to 2.34 Å in the higher temperature simulations. A possible explanation of a slightly shorter hydrogen bond length may be that at lower densities, there are decreased interactions with non-solvating waters, allowing for the coordinated waters to experience a greater polar attraction to the central molecule as there are less neighbouring waters pulling them away.

Temperature (K)	Total Water Density (g cm^{-3})	Spacing Distance (Å)	nH_2O (COM - O_w)	nH_2O (O_{oxygen} - H_w)	nH_2O (O_w - O_w)	nH-Bonds (O_w - H_w)
567	0.62	10	7.45 ± 1.12	6.41 ± 0.96	5.55 ± 0.83	1.57 ± 0.24
		20	7.69 ± 1.15	6.41 ± 0.96	5.92 ± 0.89	1.60 ± 0.24
		80	7.45 ± 1.12	6.51 ± 0.96	6.25 ± 0.64	1.61 ± 0.24
		Bulk	7.78 ± 1.17	6.60 ± 0.99	6.40 ± 0.96	1.61 ± 0.24
715	0.093	10	0.87 ± 0.14	0.76 ± 0.11	1.06 ± 0.16	1.10 ± 0.17
		20	0.93 ± 0.14	0.80 ± 0.12	1.27 ± 0.19	1.11 ± 0.17
		80	0.99 ± 0.15	0.92 ± 0.14	1.49 ± 0.22	1.17 ± 0.17
		Bulk	1.02 ± 0.15	0.93 ± 0.14	1.56 ± 0.23	1.17 ±0.17
814	0.067	10	0.72 ± 0.11	0.55 ± 0.08	0.70 ± 0.11	1.09 ± 0.16
		20	0.87 ± 0.13	0.61 ± 0.09	0.79 ± 0.12	1.06 ± 0.16
		80	0.91 ± 0.14	0.68 ± 0.10	0.97 ± 0.15	1.09 ± 0.16
		Bulk	0.96 ± 0.14	0.73 ± 0.11	0.99 ± 0.15	1.08 ± 0.16
913	0.055	10	0.63 ± 0.09	0.39 ± 0.06	0.43 ± 0.06	1.19 ± 0.18
		20	0.79 ± 0.12	0.48 ± 0.07	0.56 ± 0.08	1.04 ± 0.16
		80	0.92 ± 0.14	0.58 ± 0.09	0.70 ± 0.10	1.04 ± 0.16
		Bulk	0.99 ± 0.15	0.62 ± 0.09	0.74 ± 0.11	1.06 ± 0.16
913	0.044	10	0.40 ± 0.06	0.28 ± 0.04	0.32 ± 0.05	1.07 ± 0.16
		20	0.53 ± 0.08	0.38 ± 0.06	0.47 ± 0.07	1.03 ± 0.15
		80	0.66 ± 0.10	0.48 ± 0.07	0.56 ± 0.08	1.05 ± 0.16
		Bulk	0.67 ±0.10	0.49 ± 0.07	0.60 ± 0.09	1.05 ± 0.16

Table 1 Coordination numbers of oxygen – water and water – water solvation.

In all cases studied the hydration around both the O_2 as well as around water, have values at 80 Å of surface separation identical to that of bulk water. The subcritical 567 K simulations have the greatest fractional increase of around 4 % when transitioning from 80 Å to bulk, with the change being on average around 1 % at 913 K and 0.044 g cm^{-3}.

The numbers of hydrated water molecules around the chloride ion and the water for all $Fe(OH)_2$ configurations and bulk water systems are presented in Table 2. The numbers of coordinated waters

around chloride remains constant at around 7.7 for the subcritical condition of 567 K and 0.620 g cm^{-3}, and drops to as low as 1.5 for the 10 Å spaced system of 913 K and lowest simulated density of 0.044 g cm^{-3}.

Temperature (K)	**Density (g cm^{-3})**	**Spacing (Å)**	**n H_20 Cl^--O_w**	**n H-Bonds Cl^--H_w**	**n H_20 O_w-O_w**	**n H-Bonds O_w-H_w**
567	0.620	10	7.3 ± 1.5	5.3 ± 1.1	5.8 ± 1.2	3.1 ± 0.6
		20	7.7 ± 1.5	5.6 ± 1.1	5.7 ± 1.1	3.2 ± 0.6
		80	7.7 ± 1.5	5.8 ± 1.2	5.5 ±1.1	3.2 ± 0.6
		Bulk	7.5 ± 1.5	5.8 ± 1.2	5.4 ± 1.1	3.2 ± 0.6
715	0.093	10	4.2 ± 0.8	2.8 ± 0.6	1.8 ± 0.4	2.2 ± 0.4
		20	5.0 ± 1.0	3.2 ± 0.6	2.0 ± 0.4	2.3 ± 0.5
		80	6.0 ± 1.2	3.9 ± 0.8	2.4 ± 0.5	2.3 ± 0.5
		Bulk	6.9 ± 1.4	4.3 ± 0.9	2.4 ± 0.5	2.3 ± 0.5
814	0.067	10	2.9 ± 0.6	2.0 ± 0.4	1.2 ± 0.2	2.1 ± 0.4
		20	3.7 ± 0.7	2.4 ± 0.5	1.4 ± 0.3	2.1 ± 0.4
		80	4.9 ± 1.0	2.9 ± 0.6	1.5 ± 0.3	2.2 ± 0.4
		Bulk	5.6 ± 1.1	3.5 ± 0.7	1.5 ± 0.3	2.2 ± 0.4
913	0.055	10	2.0 ± 0.4	1.4 ± 0.3	0.8 ± 0.2	2.1 ± 0.4
		20	2.7 ± 0.5	1.8 ± 0.4	1.0 ± 0.2	2.1 ± 0.4
		80	3.8 ± 0.8	2.2 ± 0.4	1.2 ± 0.2	2.1 ± 0.4
		Bulk	4.9 ± 1.0	3.0 ± 0.6	1.2 ± 0.2	2.1 ± 0.4
913	0.044	10	1.5 ± 0.3	1.0 ± 0.2	0.6 ± 0.1	2.0 ± 0.4
		20	2.3 ± 0.5	1.5 ± 0.3	0.8 ± 0.2	2.1 ± 0.4
		80	3.3 ± 0.7	2.0 ± 0.4	0.9 ± 0.2	2.1 ± 0.4
		Bulk	4.7 ± 0.9	2.7 ± 0.5	1.0 ± 0.2	2.1 ± 0.4

Table 2 Coordination numbers of water – water and chloride – water solvation.

Coordination number was seen to decrease with increasing temperature and decreasing density and was seen to increase slightly for each system as the size of the gap was increased. Although the change in coordinated waters as gap size increased is small for the 567 K system, increasing from 7.3 to 7.7, the change becomes more pronounced in the supercritical state. This is most evident in the 913 K, 0.044 g cm^{-3} system, where the total number of waters more than doubles from 1.5 for 10 Å, to 3.3 for the 80 Å spacing.

Similarly, the number of hydrogen bonded waters around the chloride decreases with temperature as expected since the thermal energies of the molecules are too great to support extensive networking of the molecules. Chloride was seen to accept slightly over 5 hydrogen bonds in the 567 K system confined to 10 Å of surface separation. However the numbers of hydrogen bonds around the water molecules stayed almost constant in the supercritical confined systems, with a value of 2.2 for 715 K and 2.1 for both densities at 913 K.

The separation distances of the surfaces had a more dramatic effect on solvation in the high temperature simulations, with the number of waters around the chloride approximately doubling as the surface separation increased from 10 to 80 Å. The maximum coordination of water around the chloride at 80 Å of separation were close to, but slightly less than the bulk, non-confined system values.

The water-water coordination was seen to increase by only 50 % as the separation ranged from 10 to 80 Å, with the maximum coordination at 80 Å being almost the same as in the bulk system. These results suggest that at lower gas-like densities, confinement reduces the number of waters coordinated around the chloride due to the small number of waters being forced in to a tight pseudo-structured arrangement evident in the atomic density profiles shown in Figure 2.

3.3 Atomic density profiles

The atomic density profiles show the relative probability of finding an oxygen or hydrogen atom of the water, as well as the chloride ion or the atoms of the molecular oxygen at a particular position across the gap formed by the $Fe(OH)_2$ surfaces. Figure 2 a) shows the atomic density profile of molecular oxygen and water in the 567 K system with 20 Å of surface separation, and b) shows that for oxygen at 913 K and 0.044 g cm^{-3} with 10 Å of separation. Figures 2 c) and d) show the density profiles for the chloride systems with 10 Å of separation, for 567 K and 913 K and 0.044 g cm^{-3}, respectively.

Evident from the peaks for the water hydrogens and oxygen, in Figure 2 is ordering of the water molecules induced by the confining effect of the surfaces, represented by the maxima and minima of the curves. In the subcritical systems, the oxygen molecule has a delocalised position, with a negligible probability that it will be found at a specific position, relative to the ordering seen for the water molecules. Although there is a slight ordering of the oxygen molecule, evident from a magnification of the O_2 density profile (not shown) the effect is greatly reduced than the ordering seen in the water. O_2 has a preferential position in more or less the inner region of the gap. This result is consistent with the density profiles of the waters, which have the greatest probability of being situated on the surface. Although the effect may be small, the hydrophobic nature of the O_2 forces the water towards the surface, this combined with waters tendency to adsorb on the surface as well as its ordering to minimize its energy, leaves less dense regions of water corresponding to the peaks in the oxygen position.

The density profiles for both oxygen and chloride from the subcritical systems with 10 Å of separation were virtually identical and only the chloride system is shown in Figure 2 c). Both systems had a maximum in the density profile in the centre of the gap as water is forced to arrange itself to minimize its energy, and both showed a delocalised position for the solute. This ordering is mostly lost when the interfacial region reaches 20 Å of separation, shown in Figure 2 a), although at 567 K there is still evidence of hydrogen bonding to the hydroxyl groups of the surface, illustrated by the sharp peak in the density profile for the water hydrogens next to the surface. This feature is much less pronounced in the

high temperature, supercritical conditions, where the distinct hydrogen peak was effectively absent. In the 20 and 80 Å systems, the region outwards in the centre of the gap were found to be flat, suggesting that at these spacings, any ordering from confinement is lost and the water adopts a uniform, bulk like configuration.

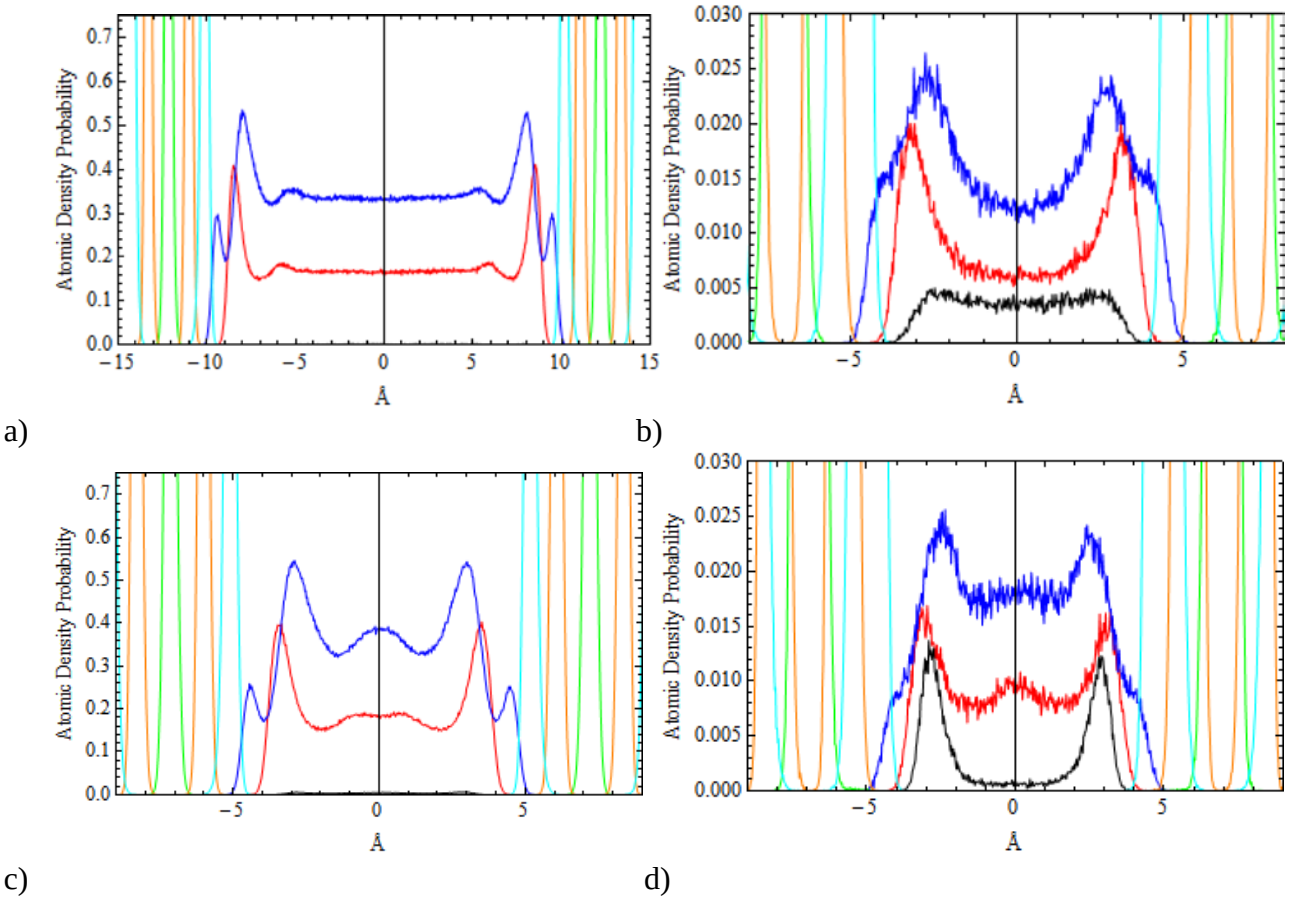

Figure 2 Atomic Density Profiles for the O_2 and Cl^- - $Fe(OH)_2$ systems. a) Density profile for O_2 at 567 K with 20 Å of surface separation, b) O_2 for 913 K and 0.044 g cm^{-3}, with 10 Å of separation c) Shows Cl^- at 567 K, with 10 Å of separation, and d) Shows the Cl^- for 913 K at 0.044 g cm^{-3}, with 10 Å of separation. Surface irons are shown in green, surface oxygen in orange, and surface hydrogens in cyan. The O_2 and Cl^- are shown in black, the water oxygen in red, and water hydrogens in blue.

Comparing the density profiles of the oxygen and chloride systems at 10 Å of separation, in Figures 2 b) and d), the chloride system has a water peak in the centre not evident in the system for oxygen. This is the result of the hydrophobic nature of the oxygen repelling water away from the centre of the gap towards the surfaces. The density profile for chloride at 913 K and 0.044 g cm^{-3} shown in d) of Figure 2, shows the opposite trend than seen with oxygen, namely that instead of the position of the solute molecule corresponding to a water minima in the centre of the gap, the chloride is most likely situated next to the surface, with its position corresponding to the water maximums. The negative charge on the chloride interacts more strongly with the surface than the O_2 and carries a larger solvation shell than the neutral oxygen molecule, resulting in the chloride weakly hydrogen bonding to the OH groups of the surface and a tendency to remain in regions of increased water density.

3.4 Diffusion coefficients

The diffusion coefficients for oxygen and chloride in all systems studied are shown in Figure 3. Figure 3a) shows those for oxygen and b) shows those for chloride. Included in Figure 3a) are also the diffusion coefficients for oxygen from our parametrized equation from reference 16. These values were obtained from the velocity autocorrelation functions and are accurate to within 15 %. The diffusion coefficients for oxygen are one to two orders of magnitude greater than those for chloride, explained by the larger solvation shell from Tables 1 and 2 above. In the oxygen system the diffusion coefficients were seen to increase as the spacing of the surfaces increased, however the opposite was observed with the chloride. This can in part be attributed to the chloride ion having a larger hydration shell at larger spacing, thereby decreasing the diffusion coefficient as the chloride must drag more water with it. Other factors influencing this behaviour of chloride diffusion can be explained by the density profiles shown in Figures 2d). The tendency of the chloride ion to carry a solvation shell contributes to this decrease in diffusion as more waters are available near the surface, effectively trapping the ion and limiting its motion.

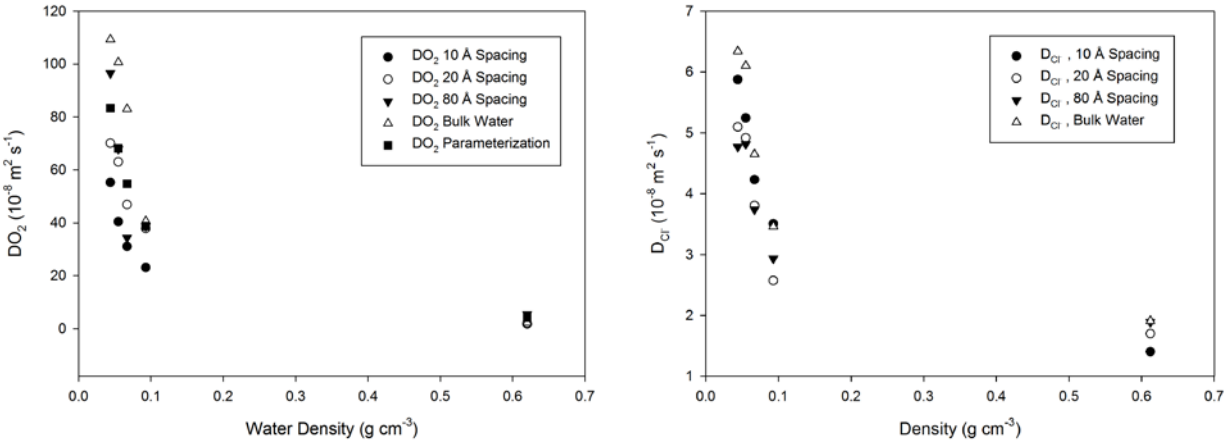

Figure 3 Diffusion Coefficients for $Fe(OH)_2$ surface systems. Figure a) shows those for oxygen and b) shows those for chloride.

This phenomenon also results in less variation of the diffusion coefficient for chloride as compared to oxygen, as the ion is most likely found near the surface, the effect of spacing is minimal and the diffusion coefficient is primarily a function of density rather than a combination of density with spacing distance as was observed for oxygen.

4. Conclusions

Classical MD simulations per performed for an oxygen molecule and chloride ion in high temperature and supercritical water in both bulk water environments and within nanometer spaced iron hydroxide surfaces. The thermodynamic state points and configurations of surface systems mimic the operating conditions and proto-cracks formed in the passivation layer of the water bearing components of the SCWR. Distinct ordering of the water molecules was observed within the surfaces spaced at 10 Å and solvation was seen to increase with surface spacing. The diffusion coefficients of oxygen increased

with gap size but chloride was seen to have the opposite behaviour, as the ion carries a much larger hydration shell as surface spacing increased. The hydrophobic nature of oxygen resulted in it being preferentially found in the centre of the gap, away from the regions of higher water density near the surfaces. Chloride was found to be situated at a surface site due to its negative charge and preference to remain more solvated, thus remaining in the region of higher water density.

5. References

[1] D. Guzonas, K. Bissonette, L. Deschenes, H. Dole, W. Cook, "Mechanistic aspects of corrosion in a supercritical water-cooled reactor", The 6th International Symposium on Supercritical Water-Cooled Reactors, Shenzhen, Guangdong, China, Paper 13086, 2013.

[2] D. Guzonas, F. Brosseau, P. Tremaine, J. Meesungnoen, J.-P. Jay-Gerin, "Water chemistry In A supercritical water–cooled pressure tube reactor", Nuclear Technology, Vol. 179, No. 2, 2012**,** pp. 205-219.

[3] O.T. Woo, J. Li, C.D. Bibby, S. Penttilä, "Corrosion mechanisms of stainless steels under SCW conditions", 6th International Symposium on SuperCritical Water-Cooled Reactors (ISSCWR-6), Shenzhen, Guangdong, China, paper 13048, 2013.

[4] I.M. Svishchev, D.T. Kallikragas, A.Y. Plugatyr, "Molecular dynamics simulations of supercritical water at the iron hydroxide surface", Journal of Supercritical Fluids, Vol. 78, 2013**,** pp. 7– 11.

[5] T.R. Allen, Y. Chen, X. Ren, K. Sridharan, L. Tan, G.S. Was, E. West, D.A. Guzonas, Comprehensive Nuclear Materials. R.J.M., K., Ed. Elsevier: Amsterdam, 2012; Vol. 5, pp 279-326.

[6] D. Guzonas, R. Novotny, "Supercritical water-cooled reactor materials - summary of research and open issues", Progress in Nuclear Energy, Vol. 77, 2014**,** pp. 361-372.

[7] G.S. Was, P. Ampornrat, G. Gupta, S. Teysseyre, E.A. West, T.R. Allen, K. Sridharan, L. Tan, Y. Chen, X. Ren, C. Pister, "Corrosion and stress corrosion cracking in supercritical water", Journal of Nuclear Materials, Vol. 371, 2007**,** pp. 176-201.

[8] R. Staehle, "Fundamental approaches to predicting stress corrosion: “Quantitative micro-nano” approach to predicting stress corrosion cracking in water cooled nuclear plants", Proceedings of the Nuclear Plant Chemistry Conference (NPC 2010), Quebec City, Canada, 2010.

[9] D. Janik, I. Janik, D.M. Bartels, "Neutron and β/γ radiolysis of water up to supercritical conditions. 1. β/γ yields for H_2, $H^{\cdot}$ atom, and hydrated electron", Journal of Physical Chemistry A, Vol. 111, 2007**,** pp. 7777-7786.

[10] D. Guzonas, L. Qiu, "Activity transport in a supercritical water-cooled reactor", The 6th International Symposium on Supercritical Water-Cooled Reactors, Shenzhen, Guangdong, China, Paper 13085, 2013.

[11] I.G. Wright, R.B. Dooley, "A review of the oxidation behaviour of structural alloys in steam", International Materials Review, Vol. 55, No. 3, 2010**,** pp. 129-167.

[12] E. Wasserman, B. Wood, J. Brodholt, "Molecular-dynamics study of the dielectric-constant of water under high-pressure and temperature conditions", Berichte der Bunsen-Gesellschaft Physical Chemistry Chemical Physics, Vol. 98, No. 7, 1994**,** pp. 906-911.

[13] Y. Guissani, B. Guillot, "A computer simulation study of the liquid-vapor coexistence curve of water", Journal of Chemical Physics, Vol. 98, 1993**,** pp. 8221-8235.

[14] A. Plugatyr, I.M. Svishchev, "Accurate thermodynamic and dielectric equations of state for high-temperature simulated water", Fluid Phase Equilibrium, Vol. 277, 2009**,** pp. 145-151.

[15] A. Plugatyr, R.A. Carvajal-Ortiz, I.M. Svishchev, "Ion-pair association constant for LiOH in supercritical water", Journal of Chemical and Engineering Data, Vol. 56, No. 9, 2011**,** pp. 3637–3642.

[16] D.T. Kallikragas, A.Y. Plugatyr, I.M. Svishchev, "High temperature diffusion coefficients for O_2, H_2, and OH in water, and for pure water", Journal of Chemical and Engineering Data, Vol. 59, 2014**,** pp. 1964−1969.

[17] R.T. Cygan, J.J. Liang, A.G. Kalinichev, "Molecular models of hydroxide, oxyhydroxide and clay phases and the development of a general force field", Journal of Physical Chemistry B, Vol. 108, 2004**,** pp. 1255–1266.

[18] R.T. Cygan, V.N. Romanov, E.M. Myshakin, "Molecular simulation of carbon dioxide capture by montmorillonite using an accurate and flexible force field", Journal of Physical Chemistry C, Vol. 116, No. 24, 2012**,** pp. 13079−13091.

[19] N. Giovambattista, P.J. Rossky, P.G. Debenedetti, "Effect of pressure on the phase behavior and structure of water confined between nanoscale hydrophobic and hydrophilic plates", Physical Review E., Vol. 73, 2006**,** pp. 041604.

[20] M.P. Allen, D.J. Tildesley, *Computer Simulation of Liquids*. Clarendon Press: New York, USA, 1989.

[21] S. Nose, "A molecular dynamics method for simulations in the canonical ensemble", Molecular Physics, Vol. 100, 2002**,** pp. 191-198.

[22] H.J.C. Berendsen, J.R. Grigera, T.P. Straatsma, "The missing term in effective pair potentials", Journal of Physical Chemistry, Vol. 91, 1987**,** pp. 6269-6271.

[23] S.J. Weiner, P.A. Kollman, D.T. Nguyen, D.A. Case, "An all atom force field for simulations of proteins and nucleic acids", Journal of Computational Chemistry, Vol. 7, No. 2, 1986**,** pp. 230-252.

[24] N. Hansen, F.A.B. Agbor, F.J. Keil, "New force fields for nitrous oxide and oxygen and their application to phase equilibria simulations", Fluid Phase Equilibrium, Vol. 259, 2007**,** pp. 180-188.